Title

Feasibility of clinical detection of cervical dysplasia using angle-resolved low coherence interferometry measurements of depth-resolved nuclear morphology.

Journal

International Journal of Cancer, 140(6)

Authors

Ho, Derek
Drake, Tyler
Smith-McCune, Karen
et al.

Publication Date

2017-03-15

DOI

10.1002/ijc.30539

Peer reviewed

HHS Public Access

Author manuscript

Int J Cancer. Author manuscript; available in PMC 2018 March 15.

Published in final edited form as:

Int J Cancer. 2017 March 15; 140(6): 1447–1456. doi:10.1002/ijc.30539.

Feasibility of clinical detection of cervical dysplasia using angle-resolved low coherence interferometry measurements of depth-resolved nuclear morphology

Derek Ho[1], **Tyler K. Drake**[1], **Karen K. Smith-McCune**[2], **Teresa M. Darragh**[3], **Loris Y. Hwang**[4,*], and **Adam Wax**[1,*]

[1]Department of Biomedical Engineering, Duke University, Durham, NC 27708, USA

[2]Department of Obstetrics, Gynecology and Reproductive Sciences, University of California, San Francisco, San Francisco, CA 94143, USA

[3]Department of Pathology, University of California, San Francisco, San Francisco, CA 94143, USA

[4]Department of Pediatrics, Division of Adolescent Medicine, University of California, San Francisco, San Francisco, CA 94118, USA

Abstract

This study sought to establish the feasibility of using *in situ* depth-resolved nuclear morphology measurements for detection of cervical dysplasia. Forty (40) enrolled patients received routine cervical colposcopy with angle-resolved low coherence interferometry (a/LCI) measurements of nuclear morphology. a/LCI scans from 63 tissue sites were compared to histopathological analysis of co-registered biopsy specimens which were classified as benign, low-grade squamous intraepithelial lesion (LSIL), or high-grade squamous intraepithelial lesion (HSIL). Results were dichotomized as dysplastic (LSIL/HSIL) versus non-dysplastic and HSIL versus LSIL/benign to determine both accuracy and potential clinical utility of a/LCI nuclear morphology measurements. Analysis of a/LCI data was conducted using both traditional Mie theory based processing and a new hybrid algorithm that provides improved processing speed to ascertain the feasibility of real-time measurements.

Analysis of depth-resolved nuclear morphology data revealed a/LCI was able to detect a significant increase in the nuclear diameter at the depth bin containing the basal layer of the epithelium for dysplastic versus non-dysplastic and HSIL versus LSIL/Benign biopsy sites (both $p < 0.001$). Both processing techniques resulted in high sensitivity and specificity (> 0.80) in identifying dysplastic biopsies and HSIL. The hybrid algorithm demonstrated a threefold decrease in processing time at a slight cost in classification accuracy. The results demonstrate the feasibility of using a/LCI as an adjunctive clinical tool for detecting cervical dysplasia and guiding the identification of optimal biopsy sites. The faster speed from the hybrid algorithm offers a promising approach for real-time clinical analysis.

Corresponding Author: Adam Wax, Department of Biomedical Engineering, Duke University, FCIEMAS 2571, 101 Science Dr., Durham, NC 27708. Phone: 919-660-5143; a.wax@duke.edu.

*Equally contributing senior authors

Conflicts of Interest

The authors declare no conflict of interest.

Keywords

cervical cancer; a/LCI; cancer screening; cancer nuclear morphology; optical biopsy

Introduction

Cervical cancer, caused by persistent human papillomavirus (HPV) infection, is the most common gynecologic cancer worldwide resulting in approximately 527,600 new diagnoses and 276,700 deaths in 2012 (1). Cervical cancer most commonly develops over the course of several years, such that early detection and treatment of cervical dysplasia (pre-cancer) is critical in preventing the progression to cancer and improving patient outcome. Traditional screening programs use cervical cytology as the primary initial screening tool for cervical dysplasia and cancer. If abnormal cytology results are found, clinicians will consider patient characteristics and formal clinical management algorithms to identify patients who should proceed to a colposcopy examination where dysplasia is diagnosed via biopsy of the most suspicious areas for histopathological analysis (2). In many Western countries, these screening programs have decreased the rates of cervical cancer by as much as 65%, significantly reducing morbidity and mortality (1).

Despite the successes of these screening techniques, they are limited in either their sensitivity, (approximately 0.54 for cytology (3) vs. 0.85 for colposcopy (4,5)) or specificity (0.69 for colposcopy vs. approximately 0.96 for cytology), with both offering limited interobserver reproducibility ($\kappa = 0.46$ for cytology (6) and $\kappa = 0.40$ for colposcopy (7)). Moreover, these techniques are resource, labor, and time intensive, requiring medical staff with the appropriate expertise and multiple patient visits over several weeks to complete the screening and diagnostic process. These limitations have inspired the development of numerous optical techniques for early detection of cervical cancer that aim to detect biochemical and structural changes in the cervical tissue indicative of neoplasia (8,9). Design of new technology requires an understanding that the vast majority of cervical dysplasia and cancers arise from persistent HPV infection at the squamo-columnar junction of the cervix, where HPV is first established among the differentiating layers of squamous metaplastic epithelium (10). HPV causes recognizable cellular changes, including increased nuclear size and density, increased nuclear to cytoplasmic ratio, and altered chromatin texture (11). Persistent HPV infection leads to progressive replacement of the epithelium with undifferentiated cells, and histologically diagnosed lesions known as low-grade squamous intraepithelial lesion (LSIL) and high-grade squamous intraepithelial lesion (HSIL) (12). Examples of optical techniques used to detect cervical dysplasia include autofluorescence microscopy (13–15), fluorescence and reflectance spectroscopy (16–20), Raman spectroscopy (21–23), optical coherence tomography (OCT) (24,25), and confocal microscopy (26–28). Some more recent advances include atomic force microscopy imaging of liquid based cytology (29), development of point-of-care tampon-based digital colposcope (30), photoacoustic imaging for detection of cervical lesions (31), fluorescence lifetime imaging of H&E tissue sections (32), and a structured illumination fiber-optic microendoscope for studying nuclear morphology in cervical columnar epithelium (33).

In this paper, we present a clinical study aimed at establishing the feasibility of using angle-resolved low coherence interferometry (a/LCI) as an optical biopsy technique for the early detection of cervical dysplasia. This technique offers unique capabilities by providing depth-resolved, nuclear morphology profiles of the cervical tissue sample, enabled by low coherence interferometry. Briefly, the technique splits light from a broadband source into a sample and reference arm. The scattered and reflected light from the sample is interfered with light from the reference arm to produce an interferogram which encodes depth resolution in the spectral fringe frequencies. The depth of the scatterer can be extracted using a Fourier transform which permits the discrimination of the scattering field from sub-surface tissue layers. This scattering field can be analyzed to extract the nuclear morphology, which can serve as a highly useful biomarker of dysplastic change (34,35). Previous studies have also used optical imaging techniques to study nuclear atypia through neoplastic progression. Quinn et al. and Pierce et al. utilized high resolution microendoscopy *in vivo* and found an increase in nucleus to cytoplasm ratio in neoplastic tissue sites (36,37). Sung et al. developed a fiber optic confocal reflectance microscope for studying nuclear morphology in cervical epithelium *in vivo* (38). Collier et al. and Drezek et al. studied changes in light scattering from pre-cancerous cervical tissues due to changes in nuclear size and chromatin optical density and texture (39,40). However, the unique capability of a/LCI to obtain quantitative nuclear morphology measurements specifically at or near the basal layer of the cervical epithelium, enables high sensitivity and specificity, by targeting measurements at the tissue site where nuclear atypia and dysplasia usually originates. This capability may support more sensitive, earlier detection of cervical dysplasia compared to other optical techniques. The diagnostic capability of a/LCI to detect nuclear abnormalities, specifically nuclear enlargement at sub-surface layers, has been demonstrated in previous studies of epithelial dysplasia including esophageal cancer *in vivo* (41), and cervical (42) and colonic cancer (43) *ex vivo*.

Nuclear morphology data is extracted computationally from a/LCI data using inverse light scattering analysis (ILSA). In this study, we used two ILSA techniques: traditional Mie theory based ILSA (44), and a new hybrid algorithm which combines Mie theory based ILSA with a continuous wavelet transform (CWT) analysis (42). While Mie theory ILSA has been shown to provide accurate nuclear morphology data, its clinical utility is limited due to long computational times, on the order of seconds. Ideally, the instrument should provide feedback to the clinician within one second for each biopsy site to provide rapid analysis and to limit the total time of an imaging session. To address this issue, we developed a hybrid algorithm that utilizes a preliminary CWT analysis, to produce a coarse estimate of the scatterer (i.e. nucleus) diameter. CWT enables faster determination of the scatterer diameter, as shown in previous studies using tissue phantoms and cell nuclei *in vitro* (45) but with some loss of accuracy and precision. The hybrid algorithm improves on the stand-alone CWT analysis by performing a fine sizing step with Mie theory ILSA over a greatly reduced database search range based on the coarse estimate. Thus, the hybrid algorithm offers a substantial improvement in processing speed compared to Mie theory ILSA, and shows potential for real-time clinical analysis (42).

This study aimed to assess the feasibility of using a/LCI depth-resolved nuclear morphology measurements to evaluate the cervical epithelium for dysplasia. We hypothesize that a/LCI

will detect nuclear enlargement in the basal layer of dysplastic cervical epithelium as compared to benign tissues. The a/LCI data were analyzed using both Mie theory ILSA and the hybrid algorithm to compare accuracy and processing speeds. We hypothesize that the hybrid algorithm will provide a significant improvement in processing time compared to Mie theory ILSA without significantly decreasing the sensitivity and specificity of the system. Proving these hypotheses demonstrates the feasibility of applying a/LCI instrumentation to evaluate cervical dysplasia and illustrates the potential real-time clinical application as a supplement to traditional cervical diagnostic techniques.

Materials and Methods

Clinical Study Protocol

We enrolled 40 women, including 33 women from the University of California, San Francisco (UCSF) Gynecologic Dysplasia Clinic and 7 healthy women from a UCSF HPV cohort study that was previously described (46). After voluntary informed consent, each woman was confirmed to be non-pregnant by urine testing, interviewed to obtain demographic and behavioral characteristics, and tested for *Chlamydia trachomatis* and *Neisseria gonorrhoeae* infection by vaginal swab for Aptima Combo2 nucleic acid amplification testing. The 33 dysplasia patients were originally referred for abnormal cytology and thus received the appropriate number of colposcopy-guided cervical biopsies as clinically indicated. The 7 healthy women each received 1 random cervical biopsy. Specifically, during a single speculum examination, a cervical cytology sample was obtained if clinically indicated and then 3% acetic acid was applied under colposcopy to identify the intended cervical biopsy sites which were recorded on a handwritten map. After the acetic acid stain faded (approximately 2–3 minutes), the a/LCI probe tip (10 mm diameter) was gently placed in contact with the tissue surface at each intended biopsy site and 100 repeated optical scans (25 milliseconds each) were recorded (total of 2.5 seconds). After removing the a/LCI probe, the acetic acid was reapplied and Tischler biopsy forceps were used to obtain tissue biopsies for histopathological analysis. The optical window at the tip of the a/LCI probe is slightly protruded, leaving a tissue indentation showing where the optical biopsy was taken. This provides visual guidance to assist the clinician in co-registering the cervical biopsies as demonstrated previously (41).

Biopsy specimens were formalin fixed and paraffin embedded in the clinical laboratory. Standard H&E stained biopsy sections were analyzed by a pathologist blinded to the a/LCI optical biopsy results. The biopsies were categorized as benign, LSIL, also known as cervical intraepithelial neoplasia-1 (CIN 1), or HSIL, also known as cervical intraepithelial neoplasia-2/3 (CIN 2/3) (12). This study was approved by the Institutional Review Boards of UCSF and Duke University.

a/LCI Instrumentation

The a/LCI design is based on a Mach-Zehnder interferometer where light from a broadband source is split into a sample and reference arm. Light in the sample arm is delivered to the tissue, and the angularly backscattered light is collected, mixed with the light in the

reference arm, detected, and analyzed to produce depth-resolved angular scattering profiles of the tissue (Figure 1).

A detailed description of the a/LCI system design and instrumentation is provided by Zhu et al. (47). Briefly, a superluminescent diode (λ = 830 nm, Superlum, Moscow, Russia) is used as the light source. The light in the sample arm is P-polarized using a polarization controller (Thorlabs, Inc., New Jersey), and propagated in a polarization maintaining fiber (Corning, Inc., New York) to the distal end of the probe tip where it is incident onto the tissue. The elastically backscattered light from the tissue is collected by a coherent fiber bundle (Schott Inc., Southbridge, MA) and mixed with path-length matched light from the reference arm. The combined signal is detected using an imaging spectrograph (SP-2150i, Princeton Instruments, Acton, MA) with a high sensitivity charge coupled device (CCD) camera (PIXIS: 100, Trenton, NJ).

To adapt the instrument for cervical imaging, a handheld wand was manufactured to enable the clinician to position the a/LCI probe tip (10 mm diameter) against the cervical epithelium (Fig 1B). A stainless steel tube in the center of the wand contains the optical fiber probe (1 mm diameter), with a 20° bend incorporated at the end of the wand to allow easier access to the cervical surface from the vaginal canal. The handle was generated from acrylonitrile butadiene styrene (ABS) via 3D printing, and the entire wand was over-molded with polyurethane to unify and stiffen the wand.

Data Processing

The a/LCI data are processed by segmenting each scan into 50 μm depth bins starting at the tissue surface and ranging to 300 μm deep. The depth bin from 200–250 μm is estimated to be the basal/parabasal layer of the epithelium, as determined from analysis of histopathology slides and features in the a/LCI scans. While the primary target of a/LCI is the basal layer of the epithelium, variations in the epithelial thickness necessitates a depth bin larger than the single cell basal layer to ensure its scattered field is captured. We refer to this depth bin as the basal/parabasal epithelial bin, which includes contributions from cells adjacent to the basal layer. The a/LCI scan is summed across scattering angles at each depth to produce a plot of signal intensity versus depth (A-scan). A-scans with insufficient signal are excluded. Reasons for poor signal quality include patient movement, probe movement, interference from cervical mucus, or poor tissue contact with the probe. All remaining scans are analyzed to determine depth resolved nuclear morphology measurements which are averaged for each biopsy site. For each scan, the angle resolved scattering profile is determined for each depth bin and analyzed to produce a nuclear morphology measurement, using the processing method discussed by Brown, et al. (44). Briefly, the scan is filtered to remove the scattering components from intercellular correlations and subcellular organelles. This isolates the scattering profile of the nucleus and obtains a nuclear morphology measurement using Mie theory ILSA or the hybrid algorithm. The nuclear morphology data are averaged across all scans for each depth bin at each biopsy site. This processing procedure is illustrated in supplemental figure 1.

In Mie theory analysis, the nuclear scattering profile is compared to a database of simulated Mie theory profiles until a best fit is found using chi-squared (χ^2) as a comparative metric.

This produces a prediction for the nuclear diameter and relative index of refraction of the cell nucleus to cytoplasm (termed the nuclear density) at each depth bin. This is repeated for all scans of sufficient quality obtained at a given biopsy site and the nuclear morphology predictions are averaged to represent the given site (more details provided by Brown, et al. (44)).

For the hybrid algorithm, a coarse sizing step using CWT based ILSA is performed prior to a fine sizing step using Mie theory ILSA. A detailed discussion of the hybrid algorithm's methodology is discussed in a previous *ex vivo* cervical tissue study (42). Briefly, peaks are observed in the CWT of the a/LCI data which connect the wavelet dilation factor to the oscillatory frequency of the angular scattering profile. These dilation factor peaks are used to estimate the size of the scatterers. Regression analysis establishes the relationship between the dilation factor peak and the size of the scatterer by application to simulated angular scattering profiles predicted by Mie theory. Thus, by taking the CWT of the a/LCI data, the dilation factor peaks are used to produce a coarse estimate of the nuclear diameter. Mie theory ILSA is then performed for a reduced database, with a range of ±1 μm around the CWT predicted nuclear diameter.

The nuclear morphology measurements from both algorithms were grouped by histopathological classification and compared. However, a/LCI measurements were not directly compared to histological image analysis, because histological tissue processing is known to produce artifacts, including the tendency for nuclei to shrink after fixing and staining. In addition, histology sections produce slices through various planes of the cell nuclei, making it difficult to produce quantitative nuclear morphology data for comparison to *in vivo* measurements.

Statistical Analysis

The independent variable was the cervical biopsy result determined by histopathology and categorized as benign, LSIL, or HSIL. We also dichotomized the histopathology using two approaches: dysplastic (LSIL and HSIL) versus non-dysplastic, and HSIL versus LSIL/benign. Although it is important to identify dysplastic biopsy sites, HSIL and LSIL have different clinical management algorithms and important clinical implications. While HSIL requires more aggressive medical intervention to remove the abnormal tissue, LSIL can resolve without treatment and is often monitored closely to ensure it does not develop into HSIL to avoid unnecessary surgical intervention. Thus, the clinical course of action for LSIL more closely resembles that of benign tissue sites. Consequently, a separate analysis was performed with the biopsies dichotomized as HSIL and LSIL/benign. The dependent variables were the nuclear diameter and density as measured by the a/LCI scans and analyzed by either the Mie theory ILSA or the hybrid algorithm.

Comparisons of two groups were conducted using two-sided Student's *t*-test, and comparisons across multiple groups were performed using ANOVA and Bonferroni post hoc analyses. Potential confounding variables included the patient's age, race (Caucasian, African-American, Asian, Mixed/Other), smoking in the past week (yes/no), and menstrual stage (periovulatory, i.e., 12 to 16 days since last menstrual period/non-periovulatory). All women in the study were negative for Chlamydia and gonorrhea infections; thus these

infections were not relevant. A multivariate regression was performed with all potential confounding variables, and statistically significant confounders were identified as follows: smoking for Mie based nuclear diameter analysis; no significant confounders for Mie based nuclear density analysis; and smoking and menstrual stage for hybrid analysis of nuclear diameter (supplemental table 1). A final multiple linear regression model was constructed which included all significant confounders, and the adjusted p-values are determined for the dependent variable in the model. P-values are reported for both unadjusted analyses and those adjusted for the relevant confounders. Sensitivity and specificity of a/LCI as a tool to identify dysplasia (HSIL/LSIL) or HSIL was determined using the optimal point on the receiver operating characteristic (ROC) curve. For hybrid analysis, the optimal point on the ROC curve was used as the nuclear diameter threshold for classifying the biopsy sites. For Mie theory ILSA, two variables (nuclear diameter and nuclear density) were used to classify the biopsy sites. Linear discriminant analysis (LDA) was used to find a linear classifier based on a linear combination of the two variables, and the optimum value of the linear classifier was found using the ROC curve. In addition, the sensitivity and specificity was determined using leave-one-out cross-validation to ensure the model does not overfit the data. Statistical analyses were performed using MATLAB, R2015a (MathWorks, Inc., Natick, MA) and R 3.2.2 (RStudio, Boston, MA).

Results

We obtained a/LCI scans of sufficient quality for analyses from 63 distinct cervical biopsy sites (benign, $n = 33$; LSIL, n = 17; HSIL, $n = 13$), derived from 29 women. We first assessed the ability of a/LCI to distinguish dysplastic (HSIL/LSIL) from non-dysplastic biopsy sites (Table 1). Using Mie theory ILSA, the nuclear diameter was determined for all depths, and the mean nuclear diameter was observed to be significantly greater for the dysplastic biopsy sites compared to the non-dysplastic biopsy sites (11.62 μm versus 8.22 μm, $p < 0.001$) at the basal/parabasal epithelial bin (200–250 μm). Lower mean nuclear density was similarly detected at the dysplastic biopsy sites compared to the non-dysplastic sites (1.042 versus 1.053, $p < 0.001$) at this depth. A scatterplot of the basal/parabasal epithelial bin nuclear morphology predictions from Mie theory ILSA are shown in Figure 2A. We observed that the optimal classification line in distinguishing dysplastic from non-dysplastic tissue sites using both nuclear density and diameter (gray dotted line) offers the same high sensitivity and specificity (1.00 and 0.97, respectively) as using nuclear diameter alone (line not shown) as the classification variable. Thus, to simplify classification, nuclear diameter alone was used as the classifier in further analyses.

Using the hybrid algorithm, a smaller but still strongly statistically significant increase in mean nuclear diameter was observed at the dysplastic biopsy sites compared to the non-dysplastic biopsy sites (10.71 μm versus 9.11 μm, $p < 0.001$) (Table 1). A scatterplot of the basal/parabasal epithelial bin nuclear morphology predictions from the hybrid algorithm are shown in Figure 2B along with the optimal nuclear diameter classification line (gray dotted line). ROC analysis resulted in an area under the curve (AUC) of 0.99 for Mie theory and 0.948 for hybrid analysis (Figure 3A). The optimal nuclear diameter threshold was determined from the ROC curves to be 9.66 μm and 10.15 μm for Mie theory ILSA and the hybrid algorithm, respectively. This produced a sensitivity and specificity of 1.0 and 0.97

respectively, for Mie theory ILSA, and 0.83 and 0.94, respectively, for the hybrid algorithm. A negative predictive value (NPV) of 1.00 and 0.86 was obtained using Mie theory ILSA and hybrid algorithm, respectively, and a positive predictive value (PPV) of 0.97 and 0.93 was obtained using Mie theory ILSA and the hybrid algorithm, respectively. Full statistical analysis of these results is presented in Table 1.

Next, we instead dichotomized the biopsy sites as HSIL and LSIL/benign, and assessed the ability of a/LCI to distinguish these categories at the basal/parabasal epithelial bin. For Mie theory ILSA, again a significantly greater nuclear diameter (12.04 μm versus 9.27 μm, $p < 0.001$) and lower nuclear density (1.041 versus 1.050, $p < 0.001$) was observed at the HSIL sites compared to the LSIL/benign sites (Table 1), and both variables are used to classify the biopsies (black dotted line, Figure 2A). The ROC for Mie theory ILSA produced an AUC of 0.914 (Figure 3B), a sensitivity of 1.0, a specificity of 0.82, a NPV of 1.00, and a PPV of 0.59. Similarly, using the hybrid algorithm for analysis, a significant increase in nuclear diameter was observed in HSIL sites (10.94 μm versus 9.11 μm, $p < 0.001$). Using the optimal nuclear diameter classification line (black dotted line, Figure 2B), the hybrid algorithm achieved an AUC of 0.871, a sensitivity of 0.92, a specificity of 0.82, a NPV of 0.97, and a PPV of 0.57. For both dichotomizations and algorithms, no change was observed in sensitivity and specificity using leave-one-out cross-validation. Full statistical analysis of these results is presented in Table 1. While high sensitivity, specificity, and NPV was retained for both algorithms in this dichotomization, a lower PPV was observed compared to that of the dysplastic vs. non-dysplastic dichotomization.

From multiple group comparison across all 3 groups (HSIL, LSIL, benign), both HSIL and LSIL have significantly higher nuclear diameter compared to benign biopsy sites for both Mie theory (both $p < 0.001$) and hybrid analysis (both $p < 0.001$) and significantly lower nuclear density for Mie theory analysis (both $p < 0.001$) (Figure 4). HSIL showed a similar trend for greater nuclear diameter ($p = 0.084$ and $p = 0.177$ for Mie theory ILSA and the hybrid algorithm, respectively) and lower nuclear density ($p = 0.062$ for Mie theory ILSA) than LSIL although this did not reach formal significance.

For calculation of data processing time, 2000 angular scattering profiles were analyzed using each algorithm and the average time per profile was calculated. Mie theory required an average of 240.7 ms to process each profile while the hybrid algorithm required 73.2 ms per profile (Table 1). Traditionally, a minimum of 10 repeated optical biopsies are taken for clinical data to sufficiently analyze each biopsy site using a/LCI (41). This corresponds to approximately 2.5 seconds and 0.75 seconds using Mie theory and the hybrid algorithm, respectively, for acquisition and processing for each optical biopsy.

Discussion

The clinical a/LCI instrument was able to detect a statistically significant increase in nuclear diameter at the basal/parabasal epithelial bin for dysplastic cervical tissue sites compared to non-dysplastic sites. This is in good agreement with our previous clinical a/LCI study on Barrett's esophagus which found an enlargement in nuclear diameter at the basal/parabasal layer depth bin of 200–300 μm to be most predictive of dysplasia (41). In addition, the high

sensitivity and specificity determined in this study are consistent with a previous a/LCI study conducted on *ex vivo* cervical tissue (42). Given the high sensitivity and specificity of both Mie theory and hybrid analysis, this pilot study demonstrates the promising clinical utility of a/LCI as an optical biopsy tool to augment traditional biopsy procedures. The high NPV of a/LCI may allow the clinician to refrain from taking a biopsy when presented with a normal nuclear morphology measurement from the optical biopsy. The clinical application of a/LCI to supplement current biopsy techniques may help clinicians to avoid acquiring biopsies from benign tissue sites, and to better locate dysplastic tissue sites.

While previous optical techniques such as high resolution microendoscopy and confocal microscopy detect changes in nuclear morphology in dysplastic cells at the superficial layers (typically less than 200 μm deep) of the epithelium, they often lack the sensitivity to detect changes in nuclear morphology in mild grade dysplasia (36–38). In this study, a/LCI was able to detect a significantly greater nuclear diameter at the basal/parabasal epithelial bin for both HSIL versus LSIL/benign, and HSIL/LSIL versus benign, using either Mie theory ILSA or the hybrid algorithm. This initial study demonstrates the ability of a/LCI to detect dysplastic tissue sites by targeting the nuclear backscattering signal from the basal/parabasal layer of the epithelium, independent of the scattering from more superficial layers. This critical targeting capability of a/LCI is not offered by other optical screening techniques; thus a/LCI is uniquely suited for clinical application to the cervical epithelium and has the potential to enhance clinical efforts towards earlier detection of cervical dysplasia.

The a/LCI approach offers advantages over other optical modalities such as fluorescence and reflectance spectroscopy which detect dysplasia by observing transformation in tissue architecture or biochemical composition, and over Raman spectroscopy which detects changes in tissue on the molecular scale. These techniques, however, do not provide information at the cellular scale, and may require the administration of exogenous contrast agents. OCT, on the other hand, has the capability of imaging the tissue epithelium in its entirety and provides an analysis of the tissue ultrastructure, but lacks the spatial resolution to measure cellular substructures, such as the nucleus. In addition, many of these modalities require an expert technician to interpret the images to make a diagnosis. The a/LCI approach has the distinct advantages of not requiring contrast agents, providing direct measurements of the nuclear morphology, and producing an independent assessment without the need for an expert technician.

A novel aspect of this study is the first evaluation of the hybrid algorithm on a clinical data set. For 10 repeated optical scans per biopsy site, the hybrid algorithm takes less than one second for analysis. Additionally, the hybrid algorithm offers over a threefold improvement in processing time compared to Mie theory ILSA which may lead to increased clinical utility of a/LCI. However, this faster processing speed comes at the cost of lower performance characteristics. In particular, use of the hybrid algorithm lowers NPV from 100% for Mie theory ILSA to 86.5%. This decrease in performance is largely due to the limitations of the CWT analysis, including a reduction in sizing resolution for larger scatterers and added error due to the relative refractive index assumption (45). In conjunction with the reduced Mie search range, this results in a constrained sizing range that has the tendency of moving towards a more central size prediction, resulting in poorer separation between the biopsy

groups. However, the faster speed could open the possibility of compensating by taking more scans at a given tissue site to improve diagnostic performance. In this study, the error of the hybrid algorithm diameter prediction compared to the Mie theory prediction decreased by an average of 1.6% for every additional scan taken. In addition, the future feasibility of real-time clinical analysis by a/LCI will rely on reasonably quick processing time to allow immediate feedback to the clinician during the patient's pelvic examination. This could be exploited as an adjunct modality to traditional screening techniques to improve detection of at-risk sites or to increase surveillance coverage of at-risk tissues.

Although neither analysis technique determined a significant difference in nuclear characteristic between LSIL and HSIL, trends of increasing diameter and decreasing nuclear density were observed for increasing severity of dysplasia. The lack of formal significance may be due to early dysplastic changes occurring in the basal layer in LSIL similar to those seen for more severe biopsy sites making the two indistinguishable. While dysplastic nuclei appear hyperchromatic in histology due to increased chromatin content, it is not fully understood why dysplastic biopsies exhibit lower nuclear density in a/LCI measurements. However, nuclear density was also found to be negatively associated with dysplasia in previous a/LCI studies (41,43). Other factors may contribute to changes in the optical density measurements including a lower density of nuclear material due to the increased nuclear volume, changes in chromatin distribution within the nuclei, and the ratio of euchromatin to heterochromatin.

A greater difference was expected in nuclear morphology closer to the surface of the epithelium (depths <200 μm) between HSIL and LSIL, but the predicted nuclear characteristics were not diagnostically significant (Supplemental figure 2). While it may be possible to use measurements from multiple layers in combination to produce a more accurate classifier, this was avoided to prevent overfitting the classification algorithm due to the limited sample size in this feasibility study. The lack of diagnostic significance may be due to confounding factors such as decreased density and sphericity of nuclei at the surface of squamous epithelium, as well as the increased susceptibility of the surface layers of the epithelium to reactive and inflammatory metaplasia. These findings are similar to those found in the clinical a/LCI esophageal study where nuclear size data collected above 200 μm were not diagnostically useful. Moreover, HPV replication occurs in the middle layers of the cervical epithelium (100–200 μm) which causes nuclear changes beginning in LSIL, making it even more difficult to distinguish differences in the nuclear characteristic of LSIL and HSIL in this layer. These factors may be contributors to the LSIL false positives, resulting in the lower PPV observed in the HSIL vs. LSIL/benign dichotomization. While the lower PPV is not ideal and may result in some unnecessary LSIL biopsies being taken, this is preferable over to a low NPV where HSIL may be missed. Despite these limitations, both the Mie theory ILSA and hybrid algorithms were able to distinguish HSIL from LSIL/benign biopsy sites with high sensitivity, specificity and NPV.

While the conclusions drawn from this study are limited by our sample size, we demonstrated the promising clinical utility of a/LCI. This initial study shows the feasibility of applying the a/LCI probe to the cervical epithelium and collecting a/LCI optical biopsy scans during a single pelvic examination in combination with traditional diagnostic

techniques. In addition, a strong relationship was found between nuclear enlargement at the basal/parabasal epithelial bin, as measured by a/LCI using Mie theory and hybrid analysis, and the presence of dysplasia in histological analysis. The data collected from this feasibility study will serve as a training set to establish the decision lines for grading biopsy sites for future prospective studies. Further advancement of the hybrid algorithm could lead to real-time processing and analysis of a/LCI scans during a patient's clinical examination. The a/LCI nuclear morphology measurements would aid the clinician in identifying dysplastic tissue sites *in vivo*. This could assist in earlier detection of tissue dysplasia, resulting in more effective medical intervention and improved patient outcome. Future work will include further refinement and validation of the clinical a/LCI instrument *in vivo* as well as the implementation of real-time processing software based on the hybrid algorithm. In addition, future technical advances will seek to enable multiple a/LCI measurements across the cervix without repositioning the probe. The main challenge of this advance is to implement an optical scanning mechanism within the probe with sufficient range to redirect the a/LCI illumination and collection point across the entire cervical epithelium to enable comprehensive screening.

Supplementary Material

Refer to Web version on PubMed Central for supplementary material.

Acknowledgments

The authors thank Anna-Barbara Moscicki for her expert consultation on the study design and for graciously facilitating patient enrollment from the UCSF HPV Cohort; and Janet Jonte and Susanna Miller Benningfield for their compassionate care in conducting the patient visits at the clinical study site.

Funding Sources

This work was supported by the National Cancer Institute (NCI) of the National Institutes of Health under grant R01-CA167421. DH is supported by the National Science Foundation Graduate Research Fellowship (DFG1106401).

Abbreviations

a/LCI	Angle-Resolved Low Coherence Interferometry
LSIL	Low-Grade Squamous Intraepithelial Lesion
HSIL	High-Grade Squamous Intraepithelial Lesion
HPV	Human Papillomavirus
OCT	Optical Coherence Tomography
ILSA	Inverse Light Scattering Analysis
CWT	Continuous Wavelet Transform
CIN 1	Cervical Intraepithelial Neoplasia-1
CIN 2/3	Cervical Intraepithelial Neoplasia-2/3

ROC	Receiver Operating Characteristic
LDA	Linear Discriminant Analysis
NPV	Negative Predictive Value
PPV	Positive Predictive Value
AUC	Area Under the Curve
CI	Confidence Interval

References

1. Torre LA, Bray F, Siegel RL, Ferlay J, Lortet-Tieulent J, Jemal A. Global Cancer Statistics, 2012. Ca-Cancer J Clin. 2015; 65(2):87–108. [PubMed: 25651787]
2. Massad LS, Einstein MH, Huh WK, Katki HA, Kinney WK, Schiffman M, et al. 2012 Updated Consensus Guidelines for the Management of Abnormal Cervical Cancer Screening Tests and Cancer Precursors. Obstet Gynecol. 2013; 121(4):829–46. [PubMed: 23635684]
3. Cuzick J, Clavel C, Petry KU, Meijer CJLM, Hoyer H, Ratnam S, et al. Overview of the European and North American studies on HPV testing in primary cervical cancer screening. Int J Cancer. 2006; 119(5):1095–101. [PubMed: 16586444]
4. Mitchell MF, Schottenfeld D, Tortolero-Luna G, Cantor SB, Richards-Kortum R. Colposcopy for the diagnosis of squamous intraepithelial lesions: A meta-analysis. Obstet Gynecol. 1998; 91(4):626–31. [PubMed: 9540955]
5. Chase DM, Kalouyan M, DiSaia PJ. Colposcopy to evaluate abnormal cervical cytology in 2008. Am J Obstet Gynecol. 2009; 200(5):472–80. [PubMed: 19375565]
6. Stoler MH, Schiffman M. Interobserver reproducibility of cervical cytologic and histologic interpretations - Realistic estimates from the ASCUS-LSIL triage study. JAMA. 2001; 285(11): 1500–05. [PubMed: 11255427]
7. Sellors JW, Nieminen P, Vesterinen E, Paavonen J. Observer variability in the scoring of colpophotographs. Obstet Gynecol. 1990; 76(6):1006–8. [PubMed: 2234707]
8. Thekkek N, Richards-Kortum R. Optical imaging for cervical cancer detection: solutions for a continuing global problem. Nat Rev Cancer. 2008; 8(9):725–31. [PubMed: 19143057]
9. Orfanoudaki IM, Kappou D, Sifakis S. Recent advances in optical imaging for cervical cancer detection. Arch Gynecol Obstet. 2011; 284(5):1197–208. [PubMed: 21800084]
10. Hwang LY, Ma YF, Shiboski SC, Farhat S, Jonte J, Moscicki AB. Active Squamous Metaplasia of the Cervical Epithelium Is Associated With Subsequent Acquisition of Human Papillomavirus 16 Infection Among Healthy Young Women. Journal of Infectious Diseases. 2012; 206(4):504–11. [PubMed: 22696500]
11. Doeberitz MV. New markers for cervical dysplasia to visualise the genomic chaos created by aberrant oncogenic papillomavirus infections. Eur J Cancer. 2002; 38(17):2229–42. [PubMed: 12441259]
12. Darragh TM, Colgan TJ, Cox JT, Heller DS, Henry MR, Luff RD, et al. The Lower Anogenital Squamous Terminology Standardization Project for HPV-associated Lesions: Background and Consensus Recommendations From the College of American Pathologists and the American Society for Colposcopy and Cervical Pathology. Int J Gynecol Pathol. 2013; 32(1):76–115. [PubMed: 23202792]
13. Drezek R, Brookner C, Pavlova I, Boiko I, Malpica A, Lotan R, et al. Autofluorescence microscopy of fresh cervical-tissue sections reveals alterations in tissue biochemistry with dysplasia. Photochem Photobiol. 2001; 73(6):636–41. [PubMed: 11421069]
14. Pavlova I, Sokolov K, Drezek R, Malpica A, Follen M, Richards-Kortum R. Microanatomical and biochemical origins of normal and precancerous cervical autofluorescence using laser-scanning

fluorescence confocal microscopy. Photochem Photobiol. 2003; 77(5):550–55. [PubMed: 12812299]

15. Weingandt H, Stepp H, Baumgartner R, Diebold J, Xiang W, Hillemanns P. Autofluorescence spectroscopy for the diagnosis of cervical intraepithelial neoplasia. Bjog-Int J Obstet Gy. 2002; 109(8):947–51.
16. Chang SK, Mirabal YN, Atkinson EN, Cox D, Malpica A, Follen M, et al. Combined reflectance and fluorescence spectroscopy for in vivo detection of cervical pre-cancer. J Biomed Opt. 2005; 10(2)
17. Nordstrom RJ, Burke L, Niloff JM, Myrtle JF. Identification of cervical intraepithelial neoplasia (CIN) using UV-excited fluorescence and diffuse-reflectance tissue spectroscopy. Laser Surg Med. 2001; 29(2):118–27.
18. Ramanujam N, Mitchell MF, Mahadevan A, Thomsen S, Silva E, Richardskortum R. Fluorescence Spectroscopy - a Diagnostic-Tool for Cervical Intraepithelial Neoplasia (Cin). Gynecol Oncol. 1994; 52(1):31–38. [PubMed: 8307499]
19. Georgakoudi I, Jacobson BC, Muller MG, Sheets EE, Badizadegan K, Carr-Locke DL, et al. NAD(P)H and collagen as in vivo quantitative fluorescent biomarkers of epithelial precancerous changes. Cancer Res. 2002; 62(3):682–7. [PubMed: 11830520]
20. Georgakoudi I, Sheets EE, Muller MG, Backman V, Crum CP, Badizadegan K, et al. Trimodal spectroscopy for the detection and characterization of cervical precancers in vivo. Am J Obstet Gynecol. 2002; 186(3):374–82. [PubMed: 11904594]
21. Jess PRT, Smith DDW, Mazilu M, Dholakia K, Riches AC, Herrington CS. Early detection of cervical neoplasia by Raman spectroscopy. Int J Cancer. 2007; 121(12):2723–28. [PubMed: 17724716]
22. Mahadevan-Jansen A, Mitchell MF, Ramanujam N, Malpica A, Thomsen S, Utzinger U, et al. Near-infrared Raman spectroscopy for in vitro detection of cervical precancers. Photochem Photobiol. 1998; 68(1):123–32. [PubMed: 9679458]
23. Utzinger U, Heintzelman DL, Mahadevan-Jansen A, Malpica A, Follen M, Richards-Kortum R. Near-infrared Raman spectroscopy for in vivo detection of cervical precancers. Appl Spectrosc. 2001; 55(8):955–59.
24. Escobar PF, Belinson JL, White A, Shakhova NM, Feldchtein FI, Kareta MV, et al. Diagnostic efficacy of optical coherence tomography in the management of preinvasive and invasive cancer of uterine cervix and vulva. Int J Gynecol Cancer. 2004; 14(3):470–74. [PubMed: 15228420]
25. Zuluaga AF, Follen M, Boiko I, Malpica A, Richards-Kortum R. Optical coherence tomography: A pilot study of a new imaging technique for noninvasive examination of cervical tissue. Am J Obstet Gynecol. 2005; 193(1):83–88. [PubMed: 16021063]
26. Collier TG, Lacy A, Malpica A, Follen M, Richards-Kortum R. Near real time confocal microscopy of amelanotic tissue: Detection of dysplasia in ex-vivo cervical tissue. P Ann Int Ieee Embs. 2002:979–81.
27. Carlson K, Pavlova I, Collier T, Descour M, Follen M, Richards-Kortum R. Confocal microscopy: Imaging cervical precancerous lesions. Gynecol Oncol. 2005; 99(3):S84–S88. [PubMed: 16143376]
28. Tan J, Quinn MA, Pyman JM, Delaney PM, McLaren WJ. Detection of cervical intraepithelial neoplasia in vivo using confocal endomicroscopy. Bjog-Int J Obstet Gy. 2009; 116(12):1663–70.
29. Guz NV, Dokukin ME, Woodworth CD, Cardin A, Sokolov I. Towards early detection of cervical cancer: Fractal dimension of AFM images of human cervical epithelial cells at different stages of progression to cancer. Nanomed-Nanotechnol. 2015; 11(7):1667–75.
30. Lam CT, Krieger MS, Gallagher JE, Asma B, Muasher LC, Schmitt JW, et al. Design of a Novel Low Cost Point of Care Tampon (POCkeT) Colposcope for Use in Resource Limited Settings. Plos One. 2015; 10(9)
31. Peng K, He L, Wang B, Xiao JY. Detection of cervical cancer based on photoacoustic imaging-the in-vitro results. Biomed Opt Express. 2015; 6(1):135–43. [PubMed: 25657882]
32. Gu J, Fu CY, Ng BK, Liu LB, Lim-Tan SK, Lee CGL. Enhancement of Early Cervical Cancer Diagnosis with Epithelial Layer Analysis of Fluorescence Lifetime Images. Plos One. 2015; 10(5)

33. Keahey PA, Tkaczyk TS, Schmeler KM, Richards-Kortum RR. Optimizing modulation frequency for structured illumination in a fiber-optic microendoscope to image nuclear morphometry in columnar epithelium. Biomed Opt Express. 2015; 6(3):870–80. [PubMed: 25798311]
34. Boone CW, Kelloff GJ, Steele VE. Natural-History of Intraepithelial Neoplasia in Humans with Implications for Cancer Chemoprevention Strategy. Cancer Res. 1992; 52(7):1651–59. [PubMed: 1551096]
35. Dey P. Cancer Nucleus: Morphology and Beyond. Diagn Cytopathol. 2010; 38(5):382–90. [PubMed: 19894267]
36. Pierce MC, Guan YY, Quinn MK, Zhang X, Zhang WH, Qiao YL, et al. A Pilot Study of Low-Cost, High-Resolution Microendoscopy as a Tool for Identifying Women with Cervical Precancer. Cancer Prev Res. 2012; 5(11):1273–79.
37. Quinn MK, Bubi TC, Pierce MC, Kayembe MK, Ramogola-Masire D, Richards-Kortum R. High-Resolution Microendoscopy for the Detection of Cervical Neoplasia in Low-Resource Settings. Plos One. 2012; 7(9)
38. Sung KB, Richards-Kortum R, Follen M, Malpica A, Liang C, Descour MR. Fiber optic confocal reflectance microscopy: a new real-time technique to view nuclear morphology in cervical squamous epithelium in vivo. Opt Express. 2003; 11(24):3171–81. [PubMed: 19471442]
39. Collier SL, Gibbs WR. Elastic scattering of pions from the three-nucleon system. Phys Rev C. 1999; 59(3):1290–97.
40. Drezek R, Guillaud M, Collier T, Boiko I, Malpica A, Macaulay C, et al. Light scattering from cervical cells throughout neoplastic progression: influence of nuclear morphology, DNA content, and chromatin texture. J Biomed Opt. 2003; 8(1):7–16. [PubMed: 12542374]
41. Terry NG, Zhu Y, Rinehart MT, Brown WJ, Gebhart SC, Bright S, et al. Detection of Dysplasia in Barrett's Esophagus With In Vivo Depth-Resolved Nuclear Morphology Measurements. Gastroenterology. 2011; 140(1):42–50. [PubMed: 20854820]
42. Ho D, Drake TK, Bentley RC, Valea FA, Wax A. Evaluation of hybrid algorithm for analysis of scattered light using ex vivo nuclear morphology measurements of cervical epithelium. Biomed Opt Express. 2015; 6(8):2755–65. [PubMed: 26309741]
43. Terry N, Zhu YZ, Thacker JKM, Migaly J, Guy C, Mantyh CR, et al. Detection of intestinal dysplasia using angle-resolved low coherence interferometry. J Biomed Opt. 2011; 16(10)
44. Brown WJ, Pyhtila JW, Terry NG, Chalut KJ, D'Amico TA, Sporn TA, et al. Review and recent development of angle-resolved low-coherence interferometry for detection of precancerous cells in human esophageal epithelium. Ieee J Sel Top Quant. 2008; 14(1):88–97.
45. Ho D, Kim S, Drake TK, Eldridge WJ, Wax A. Wavelet transform fast inverse light scattering analysis for size determination of spherical scatterers. Biomed Opt Express. 2014; 5(10):3292–304. [PubMed: 25360350]
46. Moscicki AB, Shiboski S, Hills NK, Powell KJ, Jay N, Hanson EN, et al. Regression of low-grade squamous intra-epithelial lesions in young women. Lancet. 2004; 364(9446):1678–83. [PubMed: 15530628]
47. Zhu YZ, Terry NG, Woosley JT, Shaheen NJ, Wax A. Design and validation of an angle-resolved low-coherence interferometry fiber probe for in vivo clinical measurements of depth-resolved nuclear morphology. J Biomed Opt. 2011; 16(1)

Novelty and Impact

The first clinical feasibility study of angle-resolved low coherence interferometry (a/LCI) for cervical dysplasia detection is presented. The strength of a/LCI is its depth resolution, enabling detection of increased nuclear diameter at sub-surface layers of the epithelium, yielding high sensitivity, specificity, and 100% NPV for detecting cervical dysplasia. Demonstrating feasibility of instrumentation and analysis algorithms helps justify further development of a/LCI as a real-time optical biopsy system to supplement traditional cervical cancer diagnostic techniques.

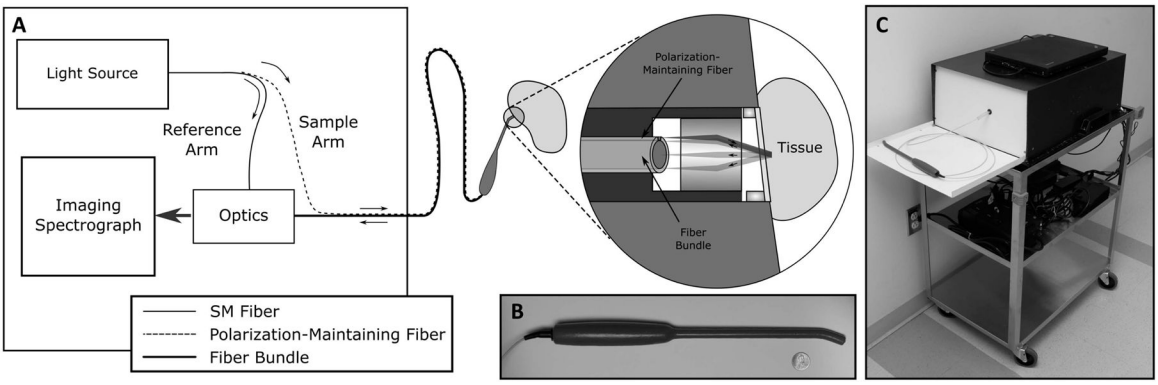

Figure 1.

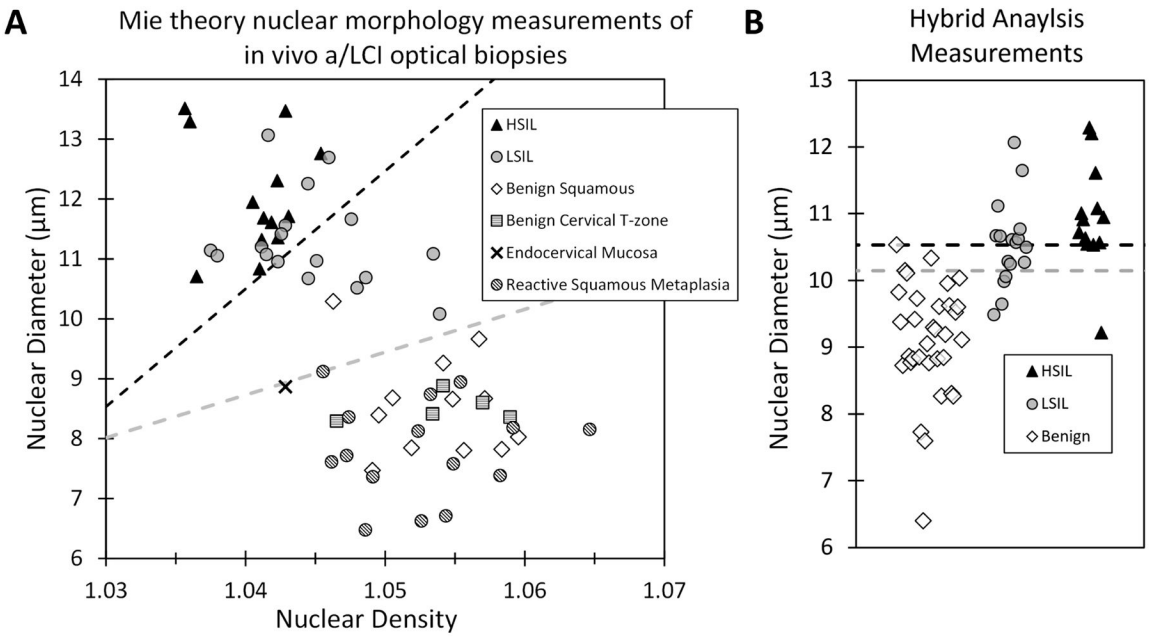

Figure 2.

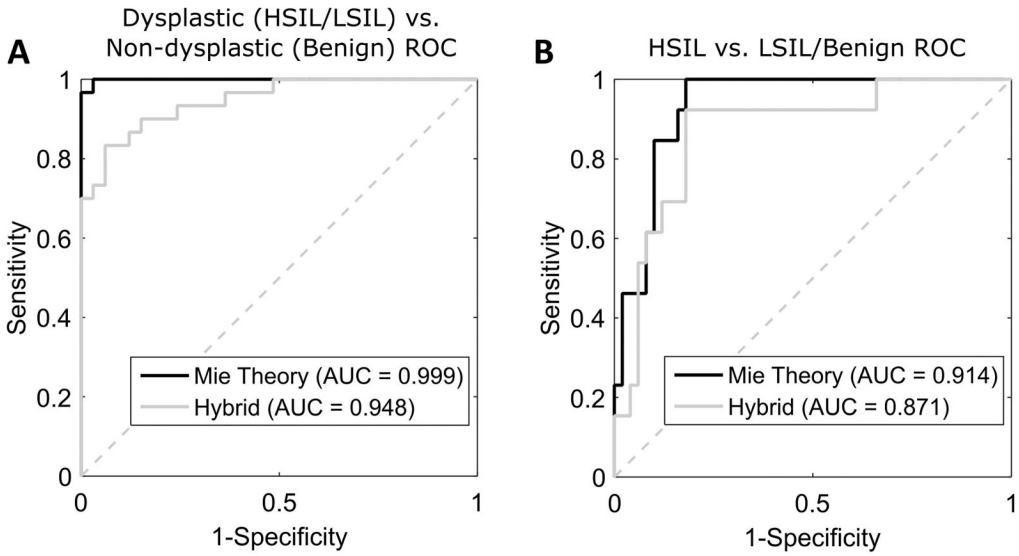

Figure 3.

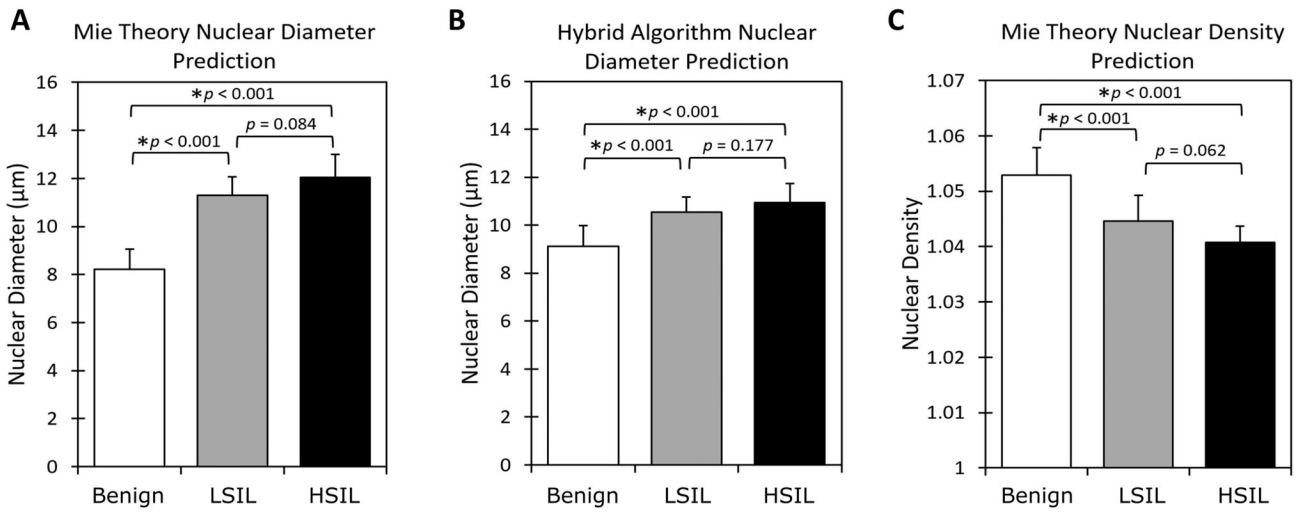

Figure 4.

Table 1

a/LCI optical biopsy results at the basal/parabasal epithelial bin (200–250 μm depth bin)

	Mie Theory ILSA	Hybrid Algorithm
Dysplastic (HSIL/LSIL) vs. Non-dysplastic (Benign)		
Nuclear diameter (μm, mean ± SD)		
Dysplastic (n = 30)	11.62 ± 0.92	10.71 ± 0.72
Non-dysplastic (n = 33)	8.22 ± 0.83	9.11 ± 0.85
Unadjusted p value	$p \ll 0.001$	$p \ll 0.001$
Adjusted p value	$p \ll 0.001$[a]	$p \ll 0.001$[b]
Nuclear Density (mean ± SD)		
Dysplastic	1.042 ± 0.004	–
Non-dysplastic	1.053 ± 0.005	–
p value	$p \ll 0.001$	–
Sensitivity [c] [95% CI]	1.00 [0.88, 1.00]	0.83 [0.65, 0.94]
Specificity [c] [95% CI]	0.97 [0.84, 1.00]	0.94 [0.79, 0.99]
NPV [95% CI]	1.00 [0.89, 1.00]	0.86 [0.71, 0.95]
PPV [95% CI]	0.97 [0.83, 1.00]	0.93 [75.7, 99.1]
ROC AUC	0.999	0.948
Accuracy	0.98 (62/63)	0.89 (56/63)
HSIL vs. LSIL/Benign		
Nuclear diameter (μm, mean ± SD)		
High Risk (n = 13)	12.04 ± 0.92	10.94 ± 0.79
Low Risk (n = 50)	9.27 ± 0.83	9.60 ± 1.04
Unadjusted p value	$p \ll 0.001$	$p \ll 0.001$
Adjusted p value	$p \ll 0.001$[a]	$p \ll 0.001$[b]
Nuclear Density (mean ± SD)		
HSIL	1.041 ± 0.003	–
LSIL/Benign	1.050 ± 0.006	–
p value	$p \ll 0.001$	–
Sensitivity [c] [95% CI]	1.00 [0.75, 1.00]	0.92 [0.64, 1.00]
Specificity [c] [95% CI]	0.82 [0.69, 0.91]	0.82 [0.69, 0.91]
NPV [95% CI]	1.00 [0.91, 1.00]	0.97 [0.87, 1.00]
PPV [95% CI]	0.59, [0.36, 0.79]	0.57 [0.34, 0.78]
ROC AUC	0.914	0.871
Accuracy	0.86 (54/63)	0.84 (53/63)
Data Processing Time (ms/profile)	240.7	73.2

[a] Adjusted for smoking

[b] Adjusted for smoking, menstrual stage

[c] Sensitivity and specificity based on optimal decision line from ROC analysis